

Pd-CeO₂ catalyst facilely derived from one-pot generated Pd@Ce-BTC for
low temperature CO oxidation

S. Xie, L. Ma

To be published in "Journal of Hazardous Materials"

March 2024

Photon Sciences

Brookhaven National Laboratory

U.S. Department of Energy

USDOE Office of Science (SC), Basic Energy Sciences (BES)

Notice: This manuscript has been authored by employees of Brookhaven Science Associates, LLC under Contract No. DE-SC0012704 with the U.S. Department of Energy. The publisher by accepting the manuscript for publication acknowledges that the United States Government retains a non-exclusive, paid-up, irrevocable, world-wide license to publish or reproduce the published form of this manuscript, or allow others to do so, for United States Government purposes.

DISCLAIMER

This report was prepared as an account of work sponsored by an agency of the United States Government. Neither the United States Government nor any agency thereof, nor any of their employees, nor any of their contractors, subcontractors, or their employees, makes any warranty, express or implied, or assumes any legal liability or responsibility for the accuracy, completeness, or any third party's use or the results of such use of any information, apparatus, product, or process disclosed, or represents that its use would not infringe privately owned rights. Reference herein to any specific commercial product, process, or service by trade name, trademark, manufacturer, or otherwise, does not necessarily constitute or imply its endorsement, recommendation, or favoring by the United States Government or any agency thereof or its contractors or subcontractors. The views and opinions of authors expressed herein do not necessarily state or reflect those of the United States Government or any agency thereof.

1 **Pd-CeO₂ catalyst facilely derived from one-pot generated Pd@Ce-BTC for low**
2 **temperature CO oxidation**

3 Shaohua Xie,^{a,†} Wei Tan,^{a,b,†} Yuhan Xu,^{a,c} Chunying Wang,^d Yuan Feng,^c Kailong Ye,^a Lu
4 Ma,^e Steven N. Ehrlich,^e Yaobin Li,^d Yan Zhang,^d Lin Dong,^c Jiguang Deng,^{c,*} Fudong
5 Liu^{a,f,*}

6 ^a Department of Civil, Environmental, and Construction Engineering, Catalysis Cluster for
7 Renewable Energy and Chemical Transformations (REACT), NanoScience Technology
8 Center (NSTC), University of Central Florida, Orlando, FL 32816, United States

9 ^b State Key Laboratory of Pollution Control and Resource Reuse, School of the Environment;
10 Jiangsu Key Laboratory of Vehicle Emissions Control, School of Chemistry and Chemical
11 Engineering; Center of Modern Analysis, Nanjing University, Nanjing 210023, China

12 ^c Beijing Key Laboratory for Green Catalysis and Separation, Key Laboratory of Beijing on
13 Regional Air Pollution Control, Key Laboratory of Advanced Functional Materials, Education
14 Ministry of China, Faculty of Environment and Life, Beijing University of Technology, Beijing
15 100124, China

16 ^d Center for Excellence in Regional Atmospheric Environment, Institute of Urban Environment,
17 Chinese Academy of Sciences, Xiamen 361021, China

18 ^e National Synchrotron Light Source II (NSLS-II), Brookhaven National Laboratory, Upton,
19 NY 11973, United States

20 ^f Department of Chemical and Environmental Engineering, University of California, Riverside,
21 California 92521, United States

22 [†] These authors contributed equally to this work.

23 ^{*} Corresponding authors. Email address: jgdeng@bjut.edu.cn (J.D.); fudong.liu@ucr.edu (F.L.)

24

25 **Abstract**

26 Due to the capacity to offer abundant catalytic sites within porous solids featuring high surface
27 areas, metal-organic frameworks (MOFs) and their derivatives have garnered considerable
28 attention as prospective catalysts in environmental catalysis. To promote the industrial
29 application of MOFs, there is an urgent need for an effective and environmental-friendly
30 preparation approach. Breaking through the limitation of the traditional two-step preparation
31 method that Pd was introduced to the already prepared Ce-BTC (Pd/Ce-BTC, BTC = 1, 3, 5
32 benzenetricarboxylate), in this work, we present a novel one-pot solvothermal method for
33 synthesizing the Pd material supported by Ce-BTC (Pd@Ce-BTC). After pyrolysis in N₂ flow
34 or air flow, Pd-CeO₂ catalysts derived from Pd@Ce-BTC exhibited much higher CO oxidation
35 activity than those from Pd/Ce-BTC. Moreover, Pd/Ce-BTC and Pd@Ce-BTC pyrolyzed in N₂
36 flow (Pd/Ce-BTC-N and Pd@Ce-BTC-N) could better catalyze the oxidation of CO than
37 Pd/Ce-BTC and Pd@Ce-BTC pyrolyzed in air flow (Pd/Ce-BTC-A and Pd@Ce-BTC-A).
38 Further characterizations revealed that the abundant surface Ce³⁺ species, rich surface adsorbed
39 oxygen species and superior redox properties were the main reasons for the superior CO
40 oxidation activity of Pd@Ce-BTC-N.

41 **Environmental Implication**

42 Precious metal catalysts derived from metal-organic frameworks (MOFs) have attracted
43 considerable attention in environmental catalysis. However, the preparation of precious metal
44 catalysts supported by MOFs typically involves multiple steps. Herein, we developed a novel
45 one-pot solvothermal method for the preparation of Pd incorporated in Ce-BTC (Pd@Ce-BTC).
46 The Pd-CeO₂ catalyst, derived from the one-pot generated Pd@Ce-BTC exhibited superior CO
47 oxidation activity comparing to the reference catalyst derived from Pd/Ce-BTC prepared
48 through a conventional two-step method. This study offers an instructive strategy for preparing
49 metal-MOF materials and their derived catalysts for potential emission control applications.

50 **Keywords**

51 Palladium catalyst, Ce-BTC, One-pot solvothermal method, CO oxidation, Surface Ce³⁺
52 species

53

54 1. Introduction

55 Due to their precisely controlled pore sizes, customizable structures, and adaptable surface
56 functionalities, metal-organic frameworks (MOFs) have been widely applied in chemical, energy
57 and environment-related fields.(Chughtai et al., 2015; Maiti et al., 2014; Ranocchiari and Bokhoven,
58 2011) Particularly, the abundant catalytic sites within high-surface-area porous structures and the
59 remarkable stability of some MOFs and their derived materials have made them promising
60 catalysts.(Freund et al., 2021; Konnerth et al., 2020; Wang and Astruc, 2020) For instance, Ikuno *et*
61 *al.* constructed Cu-oxo cluster catalysts stabilized in NU-1000 for catalyzing the oxidation of
62 methane to methanol efficiently.(Ikuno et al., 2017) An *et al.* confined the ultra-small Cu/ZnO_x
63 nanoparticles in UiO-bpy, which exhibited superior catalytic performance in the hydrogenation of
64 CO₂ to methanol.(An et al., 2017) Recently, using MOFs and MOFs-derived materials in the
65 environmental catalysis field has become a research hotspot. Among those MOFs materials, *M*-BTC
66 (*M* = Mn, Ce, Cu, Fe, *etc.*, BTC = 1, 3, 5 benzenetricarboxylate) has been widely used as important
67 precursors in the preparation of catalysts for various catalytic oxidation reactions to eliminate CO,
68 toluene, formaldehyde, and so on.(Cai et al., 2021; Chen et al., 2022; Liu et al., 2023; Su et al., 2022;
69 Zhang et al., 2021)

70 Platinum group metals (PGMs) catalysts supported by CeO₂ have been one of the most attractive
71 catalyst groups in various catalytic oxidation reactions.(Nie et al., 2017; Tan et al., 2022; Xie et al.,
72 2022; Xie et al., 2016; Xiong et al., 2021; Zhang et al., 2023) Their catalytic performance was highly
73 dependent on the states of PGMs as well as the properties of CeO₂ supports. To further tap the
74 potential of CeO₂, many strategies have been proposed to increase the surface area, control the
75 specific morphology, engineer the surface oxygen vacancies and enhance the redox capability.(Xie
76 et al., 2021) PGM catalysts on such fine-tuned CeO₂ support with proper metal-CeO₂ interactions,
77 dispersion and electronic states might exhibit superior catalytic performance in different reactions.
78 Known for the high surface area, the presence of nanosized cavities/open channels and relatively
79 low cost, Ce-BTC has been recognized as an ideal precursor for synthesizing CeO₂-based catalysts
80 with improved catalytic performance.(Chen et al., 2022; Fan et al., 2020; Fan et al., 2019; Kar et al.,
81 2020; Su et al., 2022; Zhang et al., 2021) For instance, Pd/CeO₂ catalysts derived from tetragonal
82 Ce-BTC exhibited a higher proportion of Pd⁰ and featured smaller Pd nanoparticles. These
83 characteristics resulted in the enhanced catalytic performance in CO oxidation.(Fan et al., 2020)
84 Pd/quasi-Ce-BTC synthesized through N₂ pyrolysis possessed elevated concentrations of Ce³⁺ and
85 Pd⁰, which could promote the activation of oxygen, and thus resulting in the superior catalytic
86 performance in toluene oxidation.(Su et al., 2022) Typically, these catalysts were prepared through

87 multiple steps, initially involving the synthesis of Ce-BTC followed by pretreatment or/and the
88 metal loading processes. However, such a synthetic route was intricate, costly, and less
89 environmental-friendly. In the preparation of Ce-BTC, dimethylformamide (DMF) was utilized as
90 the solvent.(Zhang et al., 2018) Additionally, it has been reported that DMF could be a reducing
91 agent in the synthesis of precious metal particles, such as Pd.(Carpenter et al., 2012) These findings
92 have inspired us to investigate the possibility of merging the preparation of MOFs with the
93 simultaneous synthesis and incorporation of precious metal particles within the pore structures of
94 MOFs. Through such a one-pot synthesis route, Ce-BTC supported metal catalysts could be
95 obtained in one step.

96 In this study, we present a one-pot solvothermal synthesis method for the *in-situ* construction of
97 Pd species within the pore structure of Ce-BTC, resulting in Pd@Ce-BTC. Serving as a reference,
98 a conventional method involving the synthesis of Ce-BTC followed by the impregnation of Pd was
99 used to prepare Pd/Ce-BTC. Both Pd@Ce-BTC and Pd/Ce-BTC materials were pyrolyzed in either
100 N₂ flow or air flow at 500 °C before use. In comparison to the Pd/CeO₂ catalysts derived from
101 conventional Pd/Ce-BTC, those prepared from one-pot synthesized Pd@Ce-BTC exhibited higher
102 Pd dispersion and enhanced CO oxidation performance. Furthermore, pyrolysis in N₂ flow was
103 found to better facilitate the formation of more surface Ce³⁺ and more surface-adsorbed oxygen
104 species on Pd/CeO₂ catalysts derived from both Pd/Ce-BTC and Pd@Ce-BTC than pyrolysis in air
105 flow. The developed one-pot solvothermal synthesis method proved to be not only straightforward,
106 efficient, and environmental-friendly, but also capable of fabricating Pd/CeO₂ catalyst with superior
107 catalytic performance in CO oxidation.

108 **2. Materials and experimental methods**

109 **2.1 Catalyst preparation**

110 Ce-BTC was synthesized through a solvothermal method reported elsewhere.(Zhang et al.,
111 2018) Typically, 10 mmol of cerium nitrate and 6.67 mmol of trimesic acid were added to 60
112 ml of DMF. After stirring at room temperature (RT) for 1 h, the solution was transferred to a
113 Teflon-lined autoclave and heated at 100 °C for 24 h with stirring. Afterwards, the product was
114 filtered once cooling to RT naturally, and washed with methanol and deionized water, followed
115 by drying in vacuum at 60 °C for 12 h.

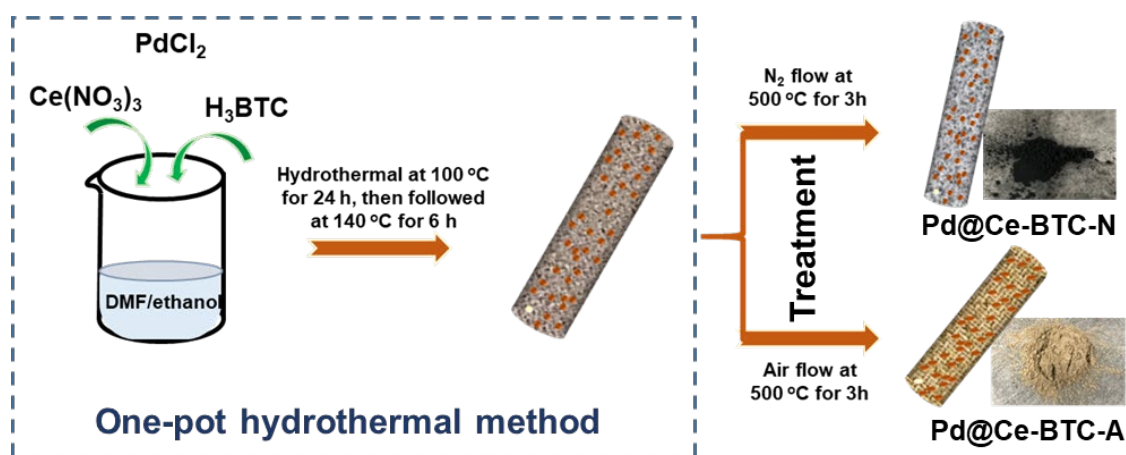
116 Pd/Ce-BTC was prepared by a solvothermal method. 2 g of as-prepared Ce-BTC was
117 dispersed in 60 ml of DMF, followed by the addition of PdCl₂ solution (1 wt.% Pd/CeO₂). After
118 stirring at RT for 1 h, the solution was transferred to a Teflon-lined autoclave and heated at
119 140 °C for 6 h with stirring. Then, the product was filtered, washed with methanol and

120 deionized water, and dried in vacuum at 60 °C for 12 h. For comparison purpose, Pd/CeO₂ was
121 also prepared via the same method except using CeO₂ as support. The CeO₂ support was
122 obtained by calcining cerium nitrate at 500 °C for 3 h.

123 Pd@Ce-BTC was prepared via a one-pot solvothermal method as illustrated in **Scheme 1**.
124 Typically, 10 mmol of cerium nitrate, 6.67 mmol of trimesic acid, and PdCl₂ solution (1 wt.%
125 Pd/CeO₂) were sequentially added to 60 ml of DMF. After stirring for 1 h, the solution was
126 transferred to a Teflon-lined autoclave and heated at 100 °C for 24 h, and then heated to 140 °C
127 and kept for another 6 h with stirring. After cooling to RT naturally, the product was filtered,
128 washed with methanol and deionized water, and vacuum-dried at 60 °C for 12 h.

129 Pd/Ce-BTC and Pd@Ce-BTC were set into a tube furnace and treated in air or N₂ flow at
130 500 °C for 3 h, and the obtained samples were suffixed with “-A” or “-N”, respectively. For
131 comparison, the Pd@Ce-BTC powder was also treated in air or N₂ flow at 800 °C for 3 h, and
132 the obtained samples were denoted as Pd@Ce-BTC-A800 or Pd@Ce-BTC-N800, respectively.
133 Pd/CeO₂ reference was treated in air flow at 800 °C for 3 h as well, and the obtained catalyst
134 was named as Pd/CeO₂-A800.

135 According to the results of inductively coupled plasma atomic emission spectroscopic (ICP-
136 AES), the real mass ratio of Pd in Pd/CeO₂, Pd/Ce-BTC-A, Pd@Ce-BTC-A, Pd/Ce-BTC-N,
137 and Pd@Ce-BTC-N to CeO₂ was 0.98, 0.95, 1.01, 0.97, and 0.93 wt.%, respectively.



139 **Scheme 1.** Schematic diagram of synthesizing Pd@Ce-BTC catalysts using a one-pot
140 hydrothermal method.

141 2.2 Catalyst characterizations

142 The detailed descriptions of catalyst characterizations by X-ray diffraction (XRD), Scanning
143 transmission electron microscopy (STEM), N₂ physisorption, X-ray photoelectron
144 spectroscopy (XPS), X-ray absorption spectroscopy (XAS), CO temperature-programmed

145 reduction (CO-TPR), O₂ temperature-programmed desorption (O₂-TPD), Raman spectroscopy,
146 and thermal gravimetric analysis (TGA) techniques can be found in the **Supplementary**
147 **material**.

148 **2.3 Catalytic performance evaluation**

149 CO oxidation test was carried out using a conventional fixed-bed flow reactor at atmospheric
150 pressure. Prior to the test, a mixture of catalyst (50 mg) and SiC (0.25 g) was loaded into a
151 quartz tube (inner diameter of 4 mm) and pretreated in 10% O₂/Ar flow at 250 °C for 30 min.
152 The feeding gas (83.3 mL·min⁻¹) was composed of 1% CO and 20% O₂, using Ar as balance,
153 corresponding to the weight hourly space velocity (WHSV) of 100,000 mL·g⁻¹·h⁻¹. The effluent
154 gas was analyzed by mass spectrometer (MS) using the *m/z* of 28, 44 and 32 for CO, CO₂ and
155 O₂, respectively. The CO conversion (*X*_{CO}) and reaction rate (*r*) on Pd catalysts were calculated
156 according to the following equations:

$$157 \quad X_{\text{CO}} (\%) = \frac{[\text{CO}]_{\text{in}} - [\text{CO}]_{\text{out}}}{[\text{CO}]_{\text{in}}} \times 100\%$$

$$158 \quad r (\mu\text{mol}\cdot\text{g}_{\text{Pd}}^{-1}\cdot\text{s}^{-1}) = \frac{F_{\text{CO}, \text{in}} \times X_{\text{CO}}}{m_{\text{Pd}}}$$

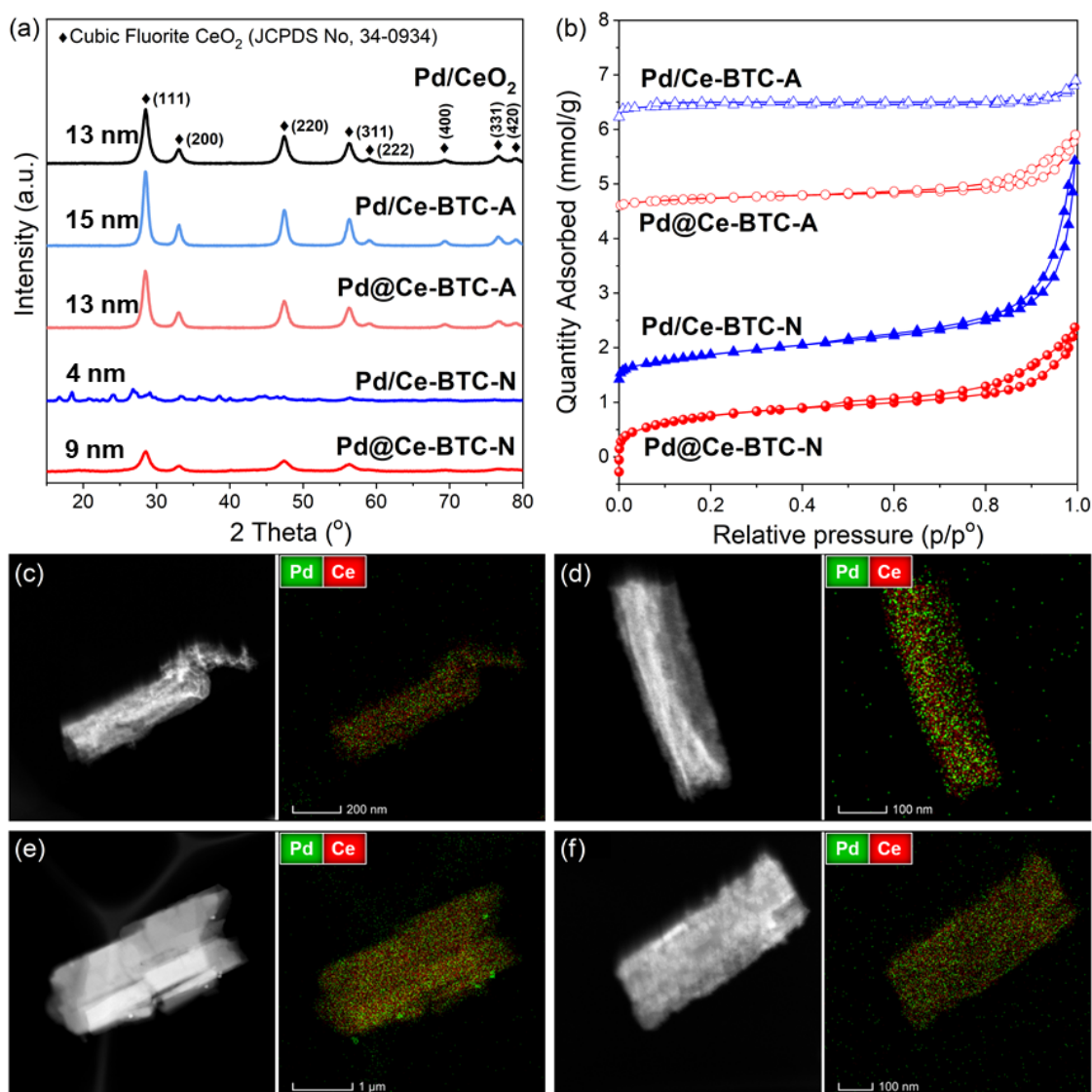
159 where [CO]_{in} and [CO]_{out} are the inlet and outlet concentrations of CO, *F*_{CO, in} is the molar flow
160 rate of CO, *X*_{CO} is the CO conversion, and *m*_{Pd} is the real mass of Pd in the catalysts.

161 **3. Results and discussion**

162 **3.1. Structural characteristics**

163 As depicted in **Fig. S1**, similar XRD patterns were observed on Ce-BTC and Pd@Ce-BTC, which
164 could be well indexed to standard Ce-BTC structure as reported.(Fan et al., 2020) In consistence
165 with Ce-BTC, Pd@Ce-BTC showed type IV isotherms (IUPAC classification) with H3-type
166 hysteresis (**Fig. S2a**). These similar XRD patterns and N₂ adsorption-desorption isotherm plots for
167 Ce-BTC and Pd@Ce-BTC indicated that the Pd species have been successfully introduced into Ce-
168 BTC without damaging its structure via this developed one-pot solvothermal method, although the
169 pore distribution of them was slightly different (**Fig. S2b**). The thermal stability and the weight loss
170 characteristics for Ce-BTC and Pd@Ce-BTC were investigated by thermogravimetric analysis
171 (TGA). As shown in **Fig. S3a**, the thermal degradation of Ce-BTC in the air flow exhibited three
172 distinct rapid weight loss phases within the temperature range of 40-800 °C. The initial weight loss
173 below 100 °C could be attributed to the loss of adsorbed and lattice-coordinated water. Subsequently,
174 from 100 to 350 °C, the second weight loss could be ascribed to the desorption and oxidation of

175 organic solvents. Lastly, the third weight loss, occurring between 350 and 800 °C, was likely
 176 associated with the combustion of the organic ligand within Ce-BTC.⁹ When subjected to the N₂
 177 flow environment, Ce-BTC exhibited two primary weight loss steps. The initial weight loss,
 178 occurring at temperatures below 500 °C, could be attributed to the desorption of water and organic
 179 solvents. Beyond 500 °C, the second step corresponded to the decomposition of organic ligand
 180 within Ce-BTC. The thermal weight loss profile of Pd@Ce-BTC closely paralleled with that of Ce-
 181 BTC in both air flow and N₂ flow, but with an overall lower weight loss (**Figs. S3b** and **S3c**). Based
 182 on the TGA results, the resulted Pd/CeO₂ catalysts for CO oxidation were precisely controlled at *ca.*
 183 1 wt.% Pd.

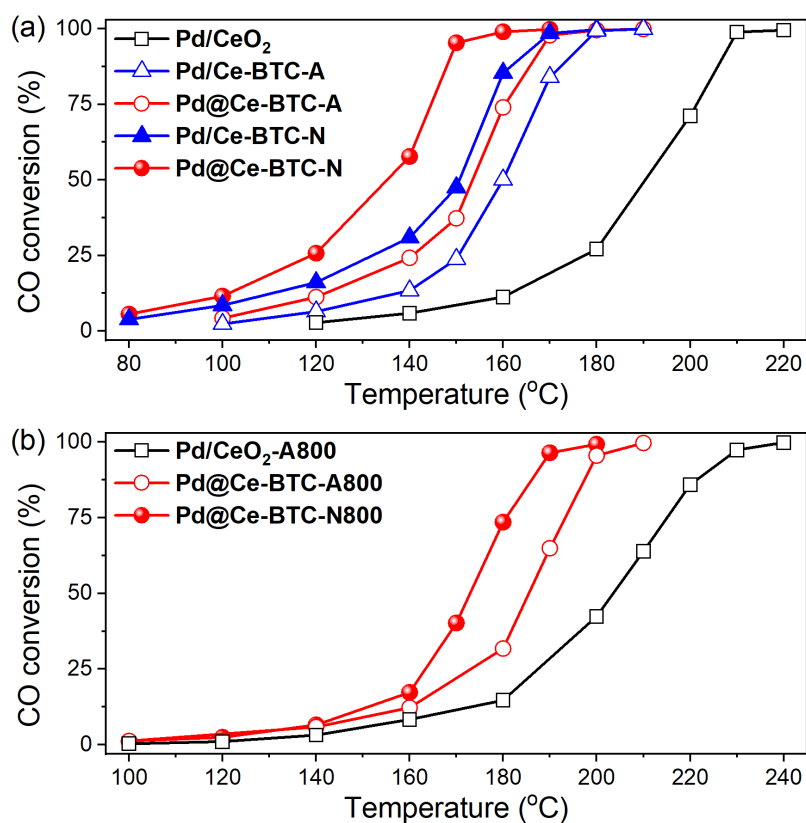


184
 185 **Fig. 1.** (a) XRD patterns and (b) N₂ adsorption-desorption isotherms for Pd catalysts; HAADF-
 186 STEM and EDS-mapping images for (c) Pd/Ce-BTC-A, (d) Pd@Ce-BTC-A, (e) Pd/Ce-BTC-N,
 187 and (f) Pd@Ce-BTC-N. The CeO₂ crystalline sizes within the catalysts are inserted in **Fig. 1a**.

188 The XRD patterns (**Fig. 1a**) for all supported Pd/CeO₂ catalysts could be attributed to the cubic
189 fluorite CeO₂ (JCPDF No. 34-0394). Comparing to the samples obtained in air flow, the XRD peaks
190 of Pd/Ce-BTC-N and Pd@Ce-BTC-N obtained in N₂ flow displayed broader full width at half
191 maximum (FWHM) of the peak, indicating the lower crystallinity of CeO₂. It should be noted that
192 there was a shift to lower angles in the XRD peaks for Pd@Ce-BTC-N and Pd@Ce-BTC-A
193 compared to those observed for Pd/CeO₂ and Pd/Ce-BTC-A (**Fig. S4**). This shift indicates a
194 lattice expansion of CeO₂ due to the presence of abundant Ce³⁺ species in the catalysts prepared
195 using the one-pot solvothermal method, potentially benefiting the CO oxidation. The lattice
196 expansion was further confirmed by the calculated lattice parameters of 0.543 nm for Pd@Ce-
197 BTC-N and 0.542 nm for Pd@Ce-BTC-A, in contrast to 0.541 nm for Pd/CeO₂ and Pd/Ce-
198 BTC-A. Comparing to Pd@Ce-BTC-N, the much weaker XRD peaks on Pd/Ce-BTC-N should be
199 due to the incomplete deligandation during the pyrolysis in N₂ flow. The crystalline size of CeO₂
200 was further calculated using Scherrer equation for confirmation. As inserted in **Fig. 1a**, the
201 crystalline sizes of CeO₂ in Pd/Ce-BTC-N (4 nm) and Pd@Ce-BTC-N (9 nm) were indeed much
202 smaller than that in Pd/Ce-BTC-A (15 nm) and Pd@Ce-BTC-A (13 nm), respectively. The results
203 of XRD were further supported by the Raman spectra (**Fig. S5**), with lower intensity of the bands
204 assigned to CeO₂ F_{2g} mode observed on Pd/Ce-BTC-N and Pd@Ce-BTC-N, which was usually
205 related to the lower crystallinity of CeO₂.^(Loridant, 2021) These results suggested that the calcination in
206 N₂ flow could benefit lowering the crystallinity of catalysts derived from Pd@Ce-BTC and Pd/Ce-
207 BTC. As illustrated in **Fig. 1b**, through the measurement of N₂ adsorption-desorption isotherms, it
208 was found that all catalysts exhibited IV isotherms with H3 hysteresis loops, suggesting the presence
209 of mesoporous structure, which was confirmed by the results of the pore size distribution (**Fig. S6**).
210 It was also found that higher specific surface area was achieved on the samples derived from the
211 pyrolysis of precursors in N₂ flow (**Table S1**), especially for Pd@Ce-BTC-N (100 m²·g⁻¹).

212 To further investigate the structure of the prepared catalysts, HAADF-STEM and EDS-mapping
213 images were collected. As shown in **Figs. 1c-1f**, all catalysts were in short rod shape, and the size
214 of CeO₂ rod in Pd@Ce-BTC-A and Pd@Ce-BTC-N was smaller than that in Pd/Ce-BTC-A and
215 Pd/Ce-BTC-N. Moreover, it was noticeable that more uniformly distributed Pd species were formed
216 on Pd@Ce-BTC-N comparing to that on Pd/Ce-BTC-N. Much smaller Pd clusters could also be
217 observed by HR-TEM images (**Fig. S7**). The observations above suggested that the one-pot
218 solvothermal synthesis method could significantly decrease the size of CeO₂ support and facilitate
219 the dispersion of Pd species.

220 3.2. Catalytic performance



221

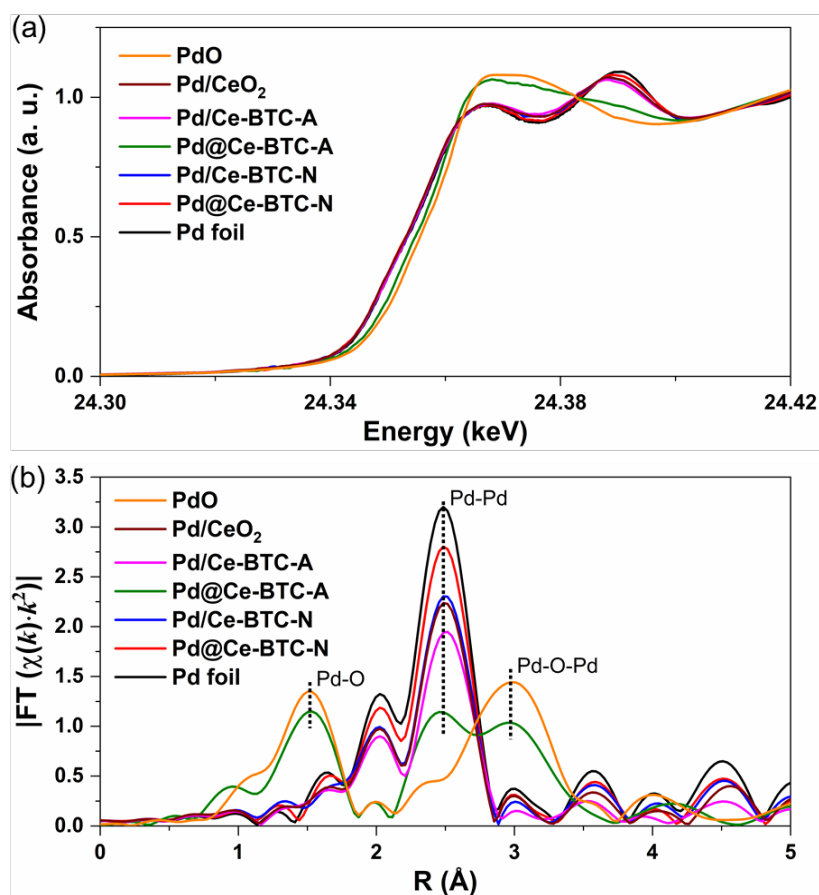
222 **Fig. 2.** CO oxidation activity on (a) Pd/CeO₂, Pd/Ce-BTC-A, Pd@Ce-BTC-A, Pd/Ce-BTC-N, and
 223 Pd@Ce-BTC-N catalysts. CO oxidation activity on (b) Pd/CeO₂-A800, Pd@Ce-BTC-A800, and
 224 Pd@Ce-BTC-N800 catalysts.

225 As a probe reaction, CO oxidation was used to evaluate the catalytic oxidation performance of the
 226 developed Pd-CeO₂ catalysts derived from Pd-Ce-BTC materials. As shown in **Fig. 2a**, the catalysts
 227 derived from both Pd/Ce-BTC and Pd@Ce-BTC performed much better than the conventional
 228 Pd/CeO₂ catalyst in CO oxidation reaction, hinting at the superiority of using Ce-BTC as the CeO₂
 229 precursor. Moreover, the catalysts derived from Pd@Ce-BTC exhibited higher activity comparing
 230 to those from Pd/Ce-BTC, underscoring the advantageous impact of the one-pot solvothermal
 231 synthesis method on enhancing the catalytic activity of Pd. Among all the catalysts, the Pd@Ce-
 232 BTC-N exhibited the highest CO oxidation activity (with T₅₀ = 135 °C, T₅₀ was the temperature at
 233 which CO conversion reached 50%). In addition, the pyrolysis atmosphere had a notable influence
 234 on the CO oxidation activity of both Pd/Ce-BTC and Pd@Ce-BTC catalysts. Notably, the catalysts
 235 pyrolyzed in N₂ flow showed higher CO oxidation activity comparing to those pyrolyzed in air flow.
 236 In comparison to the recently reported Pd-CeO₂ catalysts prepared by various methods including
 237 impregnation, the Pd@Ce-BTC-N catalyst developed in this study demonstrated superior
 238 performance (**Table S2**). The catalytic stability and thermal stability of a catalyst are crucial for

239 various operations, particularly for those conducted under high engine loads.(Nie et al., 2017)
240 Therefore, two rounds of activity testing were conducted on both Pd/Ce-BTC-N and Pd@Ce-BTC-
241 N catalysts, revealing superior catalytic stability with no observable decrease in CO oxidation
242 activity (**Fig. S8**). To further assess the thermal stability and validate the advantages of pyrolysis in
243 N₂ flow, Pd@Ce-BTC catalysts pyrolyzed in both N₂ and air flows at a high temperature of 800 °C
244 for 3 h were obtained and evaluated for CO oxidation activity. It was evident that Pd@Ce-BTC-
245 N800 exhibited higher CO oxidation activity comparing to Pd@Ce-BTC-A800 (**Fig. 2b**). Moreover,
246 Pd@Ce-BTC-A800 exhibited much higher CO oxidation activity than Pd/CeO₂-A800, indicating
247 the satisfactory stability of the catalysts derived from Pd@Ce-BTC.

248 **3.3. Oxidation states and local structure of Pd**

249 The oxidation state and local structure of Pd species on all catalysts could be determined by
250 the Pd K-edge XAS results (**Figs. 3, S9 and S10**). As depicted in **Fig. 3a**, the Pd K-edge
251 XANES patterns of Pd@Ce-BTC-N, Pd/Ce-BTC-N, Pd/Ce-BTC-A, and Pd/CeO₂ catalysts
252 were very similar to that of Pd foil, suggesting that the Pd species in these catalysts were mainly
253 in metallic state. In contrast, the XANES pattern of Pd@Ce-BTC-A was a mixture of both Pd
254 foil and PdO references, indicating that Pd species in Pd@Ce-BTC-A were partially in metallic
255 state and partially in ionic state. It was further calculated by the XANES linear combination
256 fitting analysis that the average valence state of Pd species in the Pd@Ce-BTC-N, Pd/Ce-BTC-
257 N, Pd@Ce-BTC-A, Pd/Ce-BTC-A, and Pd/CeO₂ catalysts was 0.1, 0.2, 1.7, 0.3, and 0.3,
258 respectively (**Fig. S9 and Table S3**). Such results further supported the conclusion that the Pd
259 species in Pd@Ce-BTC-N, Pd/Ce-BTC-N, Pd/Ce-BTC-A, and Pd/CeO₂ catalysts were mainly
260 in the form of Pd⁰, while those in Pd@Ce-BTC-A were mainly in the form of Pd^{δ+} (with 2 >
261 δ > 0). Considering that the Pd@Ce-BTC-A, with Pd^{δ+}, exhibited lower activity than Pd@Ce-
262 BTC-N with metallic Pd, yet showed better performance than Pd/Ce-BTC-N, Pd/Ce-BTC-A,
263 and Pd/CeO₂ in which Pd was primarily in metallic states, there was no direct correlation
264 observed between the CO oxidation activity and the oxidation valence of Pd in this catalyst
265 system. To investigate the coordination environment of Pd on different Pd-CeO₂ catalysts, the
266 EXAFS curve fitting analysis was performed (**Figs. 3b and S10, Table S4**). The observation of
267 Pd-Pd shell similar to that in Pd foil as well as the Pd-O and Pd-O-Pd shells similar to that in PdO
268 on Pd@Ce-BTC-A indicated the formation of both Pd and PdO clusters/particles. The absence of
269 Pd-O and Pd-O-Pd coordination shells and the inclusive presence of Pd-Pd coordination shell
270 on Pd@Ce-BTC-N, Pd/Ce-BTC-N, Pd/Ce-BTC-A, and Pd/CeO₂ catalysts suggested that the Pd
271 species on these catalysts were mainly in the form of metallic Pd clusters/particles.

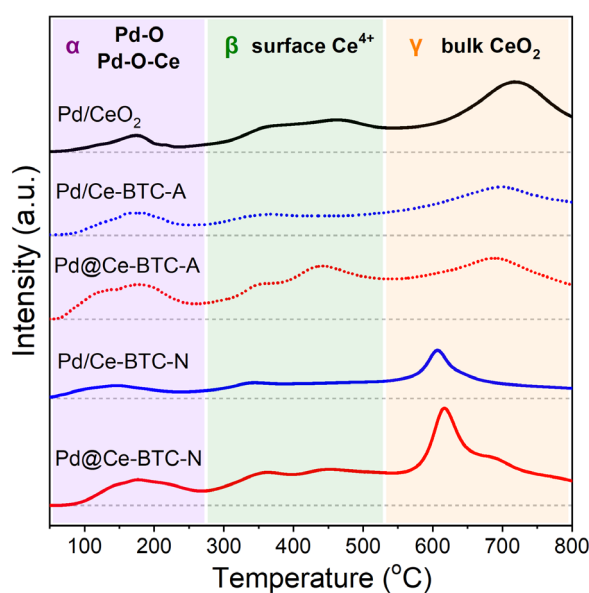


272
 273 **Fig. 3.** (a) Normalized Pd K-edge XANES and (b) Fourier transformed k^2 -weighted EXAFS
 274 oscillations in R space for Pd K-edge in Pd@Ce-BTC-N, Pd/Ce-BTC-N, Pd@Ce-BTC-A,
 275 Pd/Ce-BTC-A, and Pd/CeO₂ catalysts.

276 3.4. Catalyst reducibility

277 CO-TPR experiment was conducted to investigate the redox properties of the Pd catalysts (**Fig. 4**).
 278 The CO-consumption peaks could be divided into three zones, and zone α (50-280 °C), zone β (280-
 279 530 °C) and zone γ (530-800 °C) could be assigned to the reduction of Pd-O/Pd-O-Ce, surface Ce⁴⁺
 280 and bulk CeO₂, respectively. (Hu et al., 2016; Xie et al., 2021; Ye et al., 2019) Typically, the
 281 reducible species at low temperature range could play an important role in low temperature CO
 282 oxidation reaction. For Pd@Ce-BTC-N and Pd@Ce-BTC-A, the CO consumption peaks in zone α
 283 were much more intensive than those for Pd/CeO₂, Pd/Ce-BTC-N and Pd/Ce-BTC-A, suggesting
 284 the formation of more Pd-O and Pd-O-Ce species. This was further confirmed by the fact that a
 285 significantly higher relative CO consumption for the reduction of Pd-O/Pd-O-Ce species within
 286 Pd@Ce-BTC-N (11.5) and Pd@Ce-BTC-A (19.2) catalysts was observed comparing to that on
 287 other samples (5.1-8.2), as listed in **Table S5**. Considering the same loading of Pd on these catalysts,
 288 the formation of more Pd-O and Pd-O-Ce species could be resulted from the higher dispersion of

289 Pd on Pd@Ce-BTC as suggested by the results of EDS-mapping. As previously reported, the
 290 dispersion state and the coordination environment of Pd species could play key roles in the CO
 291 oxidation reaction.(Jeong et al., 2017; Priolkar et al., 2002; Spezzati et al., 2017; Xie et al., 2021)
 292 Our recent work also confirmed that the smaller Pd clusters on CeO₂-Al₂O₃ support exhibited better
 293 catalytic performance in CO/hydrocarbon oxidation reactions.(Xie et al., 2021) Therefore, the
 294 higher dispersion of Pd along with the superior low-temperature redox ability should have
 295 contributed to the higher CO oxidation activity on catalysts derived from Pd@Ce-BTC than those
 296 from Pd/Ce-BTC.

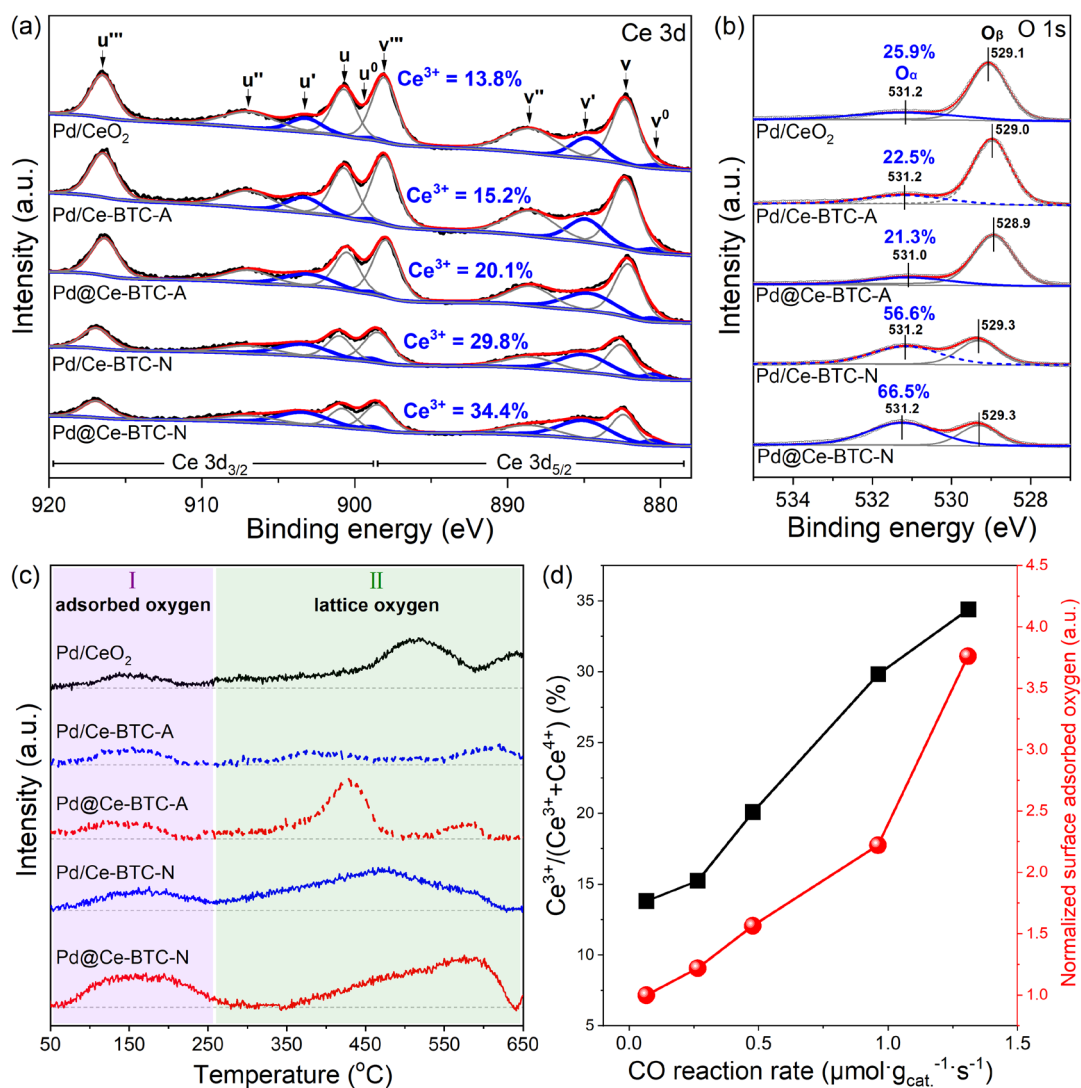


297
 298 **Fig. 4.** CO-TPR profiles for Pd/CeO₂, Pd/Ce-BTC-A, Pd@Ce-BTC-A, Pd/Ce-BTC-N and
 299 Pd@Ce-BTC-N catalysts.

300 3.5. Oxygen vacancy and oxygen species

301 **Fig. 5a** shows the Ce 3d XPS of all the catalysts, and the concentration of surface Ce³⁺ was
 302 calculated based on the fitting results.(Qi et al., 2012) All catalysts derived from Pd/Ce-BTC and
 303 Pd@Ce-BTC showed higher concentration of surface Ce³⁺ than Pd/CeO₂. Furthermore, more Ce³⁺
 304 species were observed on Pd/Ce-BTC-N (29.8%) and Pd@Ce-BTC-N (34.4%), which should be
 305 related to the lower crystallinity of CeO₂ supports with more oxygen vacancies. As widely reported,
 306 the higher concentration of surface Ce³⁺ could be beneficial for the adsorption and activation of
 307 oxygen, which therefore contributed to the improvement of catalytic oxidation performance.(Tan et
 308 al., 2021) The O 1s XPS for all the catalysts were also collected and are illustrated in **Fig. 5b**. Peak
 309 O_α and peak O_β were assigned to the surface adsorbed oxygen species and the lattice oxygen species,
 310 respectively.(Liu et al., 2018; Tan et al., 2020) As expected, much more surface adsorbed oxygen

311 species were observed on Pd/Ce-BTC-N (56.6%) and Pd@Ce-BTC-N (66.5%) than on Pd/Ce-
 312 BTC-A (22.5%), Pd@Ce-BTC-A (21.3%), and Pd/CeO₂ (25.9%), indicating that the catalysts
 313 obtained in N₂ atmosphere showed better capacity in the adsorption and activation of O₂. As
 314 previously demonstrated, the abundant surface adsorbed oxygen species could further facilitate the
 315 oxidation of CO, well explaining why the Pd/Ce-BTC-N and Pd@Ce-BTC-N catalysts showed
 316 higher CO oxidation activity than Pd/Ce-BTC-A, Pd@Ce-BTC-A, and Pd/CeO₂ counterparts. The
 317 relatively higher ratio of surface adsorbed oxygen species on Pd@Ce-BTC-N (66.5%) than that on
 318 Pd/Ce-BTC-N (56.6%) accounted for the higher CO oxidation activity achieved on the former
 319 catalyst.



320

321 **Fig. 5.** (a) Ce 3d XPS, (b) O 1s XPS, and (c) O₂-TPD profiles for Pd/CeO₂, Pd/Ce-BTC-A,
 322 Pd@Ce-BTC-A, Pd/Ce-BTC-N, and Pd@Ce-BTC-N catalysts. (d) The relationship between CO
 323 reaction rate (at 100 °C) and surface Ce³⁺ concentration as well as the normalized surface adsorbed
 324 oxygen species (the amount of surface adsorbed oxygen species on Pd/CeO₂ was normalized to 1).

O₂-TPD was conducted to further investigate the oxygen adsorption-desorption properties of Pd catalysts. As illustrated in **Fig. 5c**, two sets of oxygen desorption peaks could be observed on all catalysts. The peak I could be attributed to the desorption of oxygen species adsorbed on the surface of the catalysts, which were highly active species in catalytic oxidation reactions, while peak II could be assigned to the desorption of lattice oxygen. The normalized area of peak I was calculated and listed in **Table S1**, in which the amount of surface adsorbed oxygen species on Pd/CeO₂ reference was normalized to 1. It was noticeable that the peak I on Pd@Ce-BTC-N was much more intensive than those on other Pd catalysts, suggesting the presence of a much higher amount of surface adsorbed oxygen species on Pd@Ce-BTC-N. The results of O₂-TPD well supported the observation in O 1s XPS that more surface oxygen species were formed on Pd@Ce-BTC-N. As reported by Chen *et al.*, for the Pd-CeO₂ catalyst, the enriched surface Ce³⁺ and oxygen vacancies could facilitate the activation of O₂ to generate surface active oxygen species, which then effectively reacted with CO adsorbed on Pd sites.(Chen et al., 2018) To better reveal the relationship between surface Ce³⁺ concentrations, the amount of surface adsorbed oxygen species and the CO oxidation activity on these catalysts, the plots of Ce³⁺/(Ce³⁺ + Ce⁴⁺) ratio and the normalized surface adsorbed oxygen versus the CO reaction rate are presented in **Fig. 5d**. It was evident that the CO oxidation activity on the serial Pd-Ce-BTC derived catalysts was indeed strongly correlated to the surface Ce³⁺ concentrations and surface adsorbed oxygen. The higher concentration of surface Ce³⁺ and more abundant surface adsorbed oxygen species on Pd@Ce-BTC-N significantly contribute to its superior CO oxidation activity at low temperatures.

4. Conclusions

There is always urgent demand for simpler and more environmental-friendly preparation methods for catalytic materials, along with the enhancement of low-temperature catalytic activity. In this work, a facile one-pot solvothermal synthesis method was developed for the preparation of Pd catalysts incorporated into the CeO₂ derived from Ce-BTC (Pd@Ce-BTC). Comparing to the catalysts derived from Pd/Ce-BTC prepared by the conventional method, those derived from Pd@Ce-BTC via the one-pot solvothermal approach exhibited higher Pd dispersion and significantly improved the catalytic performance in CO oxidation. Additionally, the pyrolysis treatment conducted in N₂ flow proved to be more favorable for obtaining more efficient Pd-CeO₂ catalyst comparing to the pyrolysis treatment in air flow. Among all the investigated catalysts, the Pd@Ce-BTC-N pyrolyzed in N₂ flow showed exceptional catalytic activity for CO oxidation, due to its higher Pd dispersion and more surface Ce³⁺ species and adsorbed oxygen species. This work provides an instructive strategy for the preparation of metal-MOF materials and their derived

358 catalysts aimed at the more effective control of industrial or automotive emissions.

359 **CRedit authorship contribution statement**

360 **Shaohua Xie, Wei Tan:** Investigation, Writing – original draft, Writing – review & editing,
361 Visualization. **Yuhan Xu:** Investigation, Formal analysis, Visualization. **Chunying Wang,**
362 **Yuan Feng, Kailong Ye:** Investigation, Formal analysis. **Lu Ma, Steven N. Ehrlich, Yaobin**
363 **Li, Yan Zhang, Lin Dong:** Investigation, Resources. **Jiguang Deng, Fudong Liu:**
364 Conceptualization, Supervision, Funding acquisition, Writing – review & editing. All authors
365 read the manuscript and approved the submission.

366 **Declaration of Competing Interest**

367 The authors declare no competing financial interest.

368 **Data Availability**

369 Data will be made available on request.

370 **Acknowledgement**

371 This work was supported by the Startup Fund (F. L.) from the University of Central Florida
372 (UCF) and the NSF-PREM grant (DMR-2121953). J. D. thanks the support from National
373 Natural Science Foundation of China (22106007), Key Science and Technology Projects of
374 Beijing Municipal Education Commission (KZ202210005011), and Natural Science
375 Foundation of Hebei Province (B2021208033). S. X. thanks the support from the Preeminent
376 Postdoctoral Program (P3) at UCF. W. T. thanks the support from National Natural Science
377 Foundation of China (22306090). This research used beamline 7-BM (QAS) of the National
378 Synchrotron Light Source II (NSLS-II), a U.S. Department of Energy (DOE) Office of Science
379 User Facility operated for the DOE Office of Science by Brookhaven National Laboratory
380 (BNL) under Contract No. DE-SC0012704.

381 **Appendix A. Supporting information**

382 Supplementary data associated with this article can be found in the online version at
383 [doi:10.1016/j.jhazmat.2023.xxxxxx](https://doi.org/10.1016/j.jhazmat.2023.xxxxxx).

384 Details on characterization methods, surface area, pore volume, surface chemical states, XRD,
385 N₂ adsorption-desorption isotherm and pore size distribution, TGA, Raman spectra, TEM
386 images, and EXAFS fitting results (PDF)

387

- 389 An, B., Zhang, J., Cheng, K., Ji, P., Wang, C., Lin, W., 2017. Confinement of ultrasmall
390 Cu/ZnO_x nanoparticles in metal–organic frameworks for selective methanol synthesis from
391 catalytic hydrogenation of CO₂. *J. Am. Chem. Soc.* 139(10), 3834-3840.
392 <https://doi.org/10.1021/jacs.7b00058>.
- 393 Cai, D., Chen, B., Huang, Z., Zeng, X., Xiao, J., Zhou, S.F., Zhan, G., 2021. Metal oxide/CeO₂
394 nanocomposites derived from Ce-benzene tricarboxylate (Ce-BTC) adsorbing with metal
395 acetylacetonate complexes for catalytic oxidation of carbon monoxide. *RSC Adv.* 11(34),
396 21057-21065. <https://doi.org/10.1039/d1ra03319k>.
- 397 Carpenter, M.K., Moylan, T.E., Kukreja, R.S., Atwan, M.H., Tessema, M.M., 2012.
398 Solvothermal synthesis of platinum alloy nanoparticles for oxygen reduction
399 electrocatalysis. *J. Am. Chem. Soc.* 134(20), 8535-8542.
400 <https://doi.org/10.1021/ja300756y>.
- 401 Chen, B., Zeng, X., Liu, Y., Xiao, F., Huang, M., Bing Tan, K., Cai, D., Huang, J., Zhan, G.,
402 2022. Thermal decomposition kinetics of *M*-BTC (*M* = Cu, Co, Zn, and Ce) and
403 *M*-BTC/Pt composites under oxidative and reductive environments. *Chem. Eng. J.* 450.
404 <https://doi.org/10.1016/j.cej.2022.138470>.
- 405 Chen, Y., Chen, J., Qu, W., George, C., Aouine, M., Vernoux, P., Tang, X., 2018. Well-defined
406 palladium–ceria interfacial electronic effects trigger CO oxidation. *Chem. Commun.*
407 54(72), 10140-10143. <https://doi.org/10.1039/C8CC04935A>.
- 408 Chughtai, A.H., Ahmad, N., Younus, H.A., Laypkov, A., Verpoort, F., 2015. Metal–organic
409 frameworks: versatile heterogeneous catalysts for efficient catalytic organic
410 transformations. *Chem. Soc. Rev.* 44(19), 6804-6849.
411 <https://doi.org/10.1039/C4CS00395K>.
- 412 Fan, L., Wang, K., Xu, K., Liang, Z., Wang, H., Zhou, S.F., Zhan, G., 2020. Structural
413 isomerism of two Ce-BTC for fabricating Pt/CeO₂ nanorods toward low-temperature CO
414 oxidation. *Small* 16(40), e2003597. <https://doi.org/10.1002/sml.202003597>.
- 415 Fan, L., Zhao, F., Huang, Z., Chen, B., Zhou, S.-F., Zhan, G., 2019. Partial deligandation of
416 *M*/Ce-BTC nanorods (*M* = Au, Cu, Au-Cu) with “Quasi-MOF” structures towards
417 improving catalytic activity and stability. *Appl. Catal. A: Gen.* 572, 34-43.
418 <https://doi.org/10.1016/j.apcata.2018.12.021>.
- 419 Freund, R., Zaremba, O., Arnauts, G., Ameloot, R., Skorupskii, G., Dinca, M., Bavykina, A.,
420 Gascon, J., Ejsmont, A., Goscianska, J., Kalmutzki, M., Lachelt, U., Ploetz, E., Diercks,
421 C.S., Wuttke, S., 2021. The current status of MOF and COF applications. *Angew. Chem.*
422 *Int. Ed.* 60(45), 23975-24001. <https://doi.org/10.1002/anie.202106259>.
- 423 Hu, Z., Liu, X., Meng, D., Guo, Y., Guo, Y., Lu, G., 2016. Effect of ceria crystal plane on the
424 physicochemical and catalytic properties of Pd/ceria for CO and propane oxidation. *ACS*
425 *Catal.* 6(4), 2265-2279. <https://doi.org/10.1021/acscatal.5b02617>.
- 426 Ikuno, T., Zheng, J., Vjunov, A., Sanchez-Sanchez, M., Ortuño, M.A., Pahls, D.R., Fulton, J.L.,
427 Camaioni, D.M., Li, Z., Ray, D., Mehdi, B.L., Browning, N.D., Farha, O.K., Hupp, J.T.,
428 Cramer, C.J., Agliardi, L., Lercher, J.A., 2017. Methane oxidation to methanol catalyzed
429 by Cu-Oxo clusters stabilized in NU-1000 metal–organic framework. *J. Am. Chem. Soc.*
430 139(30), 10294-10301. <https://doi.org/10.1021/jacs.7b02936>.
- 431 Jeong, H., Bae, J., Han, J.W., Lee, H., 2017. Promoting effects of hydrothermal treatment on
432 the activity and durability of Pd/CeO₂ catalysts for CO oxidation. *ACS Catal.* 7(10), 7097-
433 7105. <https://doi.org/10.1021/acscatal.7b01810>.
- 434 Kar, A.K., Kaur, S.P., Kumar, T.J.D., Srivastava, R., 2020. Efficient hydrogenolysis of aryl
435 ethers over Ce-MOF supported Pd NPs under mild conditions: mechanistic insight using
436 density functional theoretical calculations. *Catal. Sci. Technol.* 10(20), 6892-6901.

437 <https://doi.org/10.1039/d0cy01279c>.

438 Konnerth, H., Matsagar, B.M., Chen, S.S., Prechtel, M.H.G., Shieh, F.-K., Wu, K.C.W., 2020.

439 Metal-organic framework (MOF)-derived catalysts for fine chemical production. *Coord.*

440 *Chem. Rev.* 416, 213319. <https://doi.org/10.1016/j.ccr.2020.213319>.

441 Liu, F., Shan, W., Lian, Z., Liu, J., He, H., 2018. The smart surface modification of Fe₂O₃ by

442 WO_x for significantly promoting the selective catalytic reduction of NO_x with NH₃. *Appl.*

443 *Catal., B* 230, 165-176. <https://doi.org/https://doi.org/10.1016/j.apcatb.2018.02.052>.

444 Liu, Y., Jie, W., Liu, F., Liu, Q., Qiu, M., Gong, X., Hu, J., Gong, L., 2023. Effect of Ce-BTC

445 precursor morphology on CuO/CeO₂ catalysts for CO preferential oxidation in H₂-rich gas.

446 *Solid State Sciences* 139, 107182.

447 <https://doi.org/10.1016/j.solidstatesciences.2023.107182>.

448 Loridant, S., 2021. Raman spectroscopy as a powerful tool to characterize ceria-based catalysts.

449 *Catal. Today* 373, 98-111. <https://doi.org/https://doi.org/10.1016/j.cattod.2020.03.044>.

450 Maiti, S., Pramanik, A., Mahanty, S., 2014. Extraordinarily high pseudocapacitance of metal

451 organic framework derived nanostructured cerium oxide. *Chem. Commun.* 50(79), 11717-

452 11720. <https://doi.org/10.1039/C4CC05363J>.

453 Nie, L., Mei, D., Xiong, H., Peng, B., Ren, Z., Hernandez, X.I.P., DeLaRiva, A., Wang, M.,

454 Engelhard, M.H., Kovarik, L., Datye, A.K., Wang, Y., 2017. Activation of surface lattice

455 oxygen in single-atom Pt/CeO₂ for low-temperature CO oxidation. *Science* 358, 1419-1423.

456 <https://doi.org/10.1126/science.aao2109>.

457 Priolkar, K.R., Bera, P., Sarode, P.R., Hegde, M.S., Emura, S., Kumashiro, R., Lalla, N.P.,

458 2002. Formation of Ce_{1-x}Pd_xO_{2-δ} solid solution in combustion-synthesized Pd/CeO₂

459 catalyst: XRD, XPS, and EXAFS investigation. *Chem. Mater.* 14(5), 2120-2128.

460 <https://doi.org/10.1021/cm0103895>.

461 Qi, L., Yu, Q., Dai, Y., Tang, C., Liu, L., Zhang, H., Gao, F., Dong, L., Chen, Y., 2012.

462 Influence of cerium precursors on the structure and reducibility of mesoporous CuO-CeO₂

463 catalysts for CO oxidation. *Appl. Catal., B* 119-120, 308-320.

464 <https://doi.org/https://doi.org/10.1016/j.apcatb.2012.02.029>.

465 Ranocchiari, M., Bokhoven, J.A.v., 2011. Catalysis by metal-organic frameworks:

466 fundamentals and opportunities. *Phys. Chem. Chem. Phys.* 13(14), 6388-6396.

467 <https://doi.org/10.1039/C0CP02394A>.

468 Spezzati, G., Su, Y., Hofmann, J.P., Benavidez, A.D., DeLaRiva, A.T., McCabe, J., Datye,

469 A.K., Hensen, E.J.M., 2017. Atomically dispersed Pd-O species on CeO₂(111) as highly

470 active sites for low-temperature CO oxidation. *ACS Catal.* 7(10), 6887-6891.

471 <https://doi.org/10.1021/acscatal.7b02001>.

472 Su, C., Li, Z., Mao, M., Ye, W., Zhong, J., Ren, Q., Cheng, H., Huang, H., Fu, M., Wu, J., Hu,

473 Y., Ye, D., Xu, H., 2022. Unraveling specific role of carbon matrix over Pd/quasi-Ce-MOF

474 facilitating toluene enhanced degradation. *J. Rare Earths* 40(11), 1751-1762.

475 <https://doi.org/10.1016/j.jre.2021.09.017>.

476 Tan, W., Wang, J., Li, L., Liu, A., Song, G., Guo, K., Luo, Y., Liu, F., Gao, F., Dong, L., 2020.

477 Gas phase sulfation of ceria-zirconia solid solutions for generating highly efficient and SO₂

478 resistant NH₃-SCR catalysts for NO removal. *J. Hazard. Mater.* 388, 121729.

479 <https://doi.org/https://doi.org/10.1016/j.jhazmat.2019.121729>.

480 Tan, W., Xie, S., Le, D., Diao, W., Wang, M., Low, K.B., Austin, D., Hong, S., Gao, F., Dong,

481 L., Ma, L., Ehrlich, S.N., Rahman, T.S., Liu, F., 2022. Fine-tuned local coordination

482 environment of Pt single atoms on ceria controls catalytic reactivity. *Nat. Commun.* 13(1),

483 7070. <https://doi.org/10.1038/s41467-022-34797-2>.

484 Tan, W., Xie, S., Wang, X., Wang, C., Li, Y., Shaw, T.E., Ma, L., Ehrlich, S.N., Liu, A., Ji, J.,

485 Gao, F., Dong, L., Liu, F., 2021. Highly efficient Pt catalyst on newly designed CeO₂-ZrO₂-

486 Al₂O₃ support for catalytic removal of pollutants from vehicle exhaust. *Chem. Eng. J.* 426,

487 131855. <https://doi.org/https://doi.org/10.1016/j.cej.2021.131855>.

488 Wang, Q., Astruc, D., 2020. State of the art and prospects in metal-organic framework (MOF)-
489 based and MOF-derived nanocatalysis. *Chem. Rev.* 120(2), 1438-1511.
490 <https://doi.org/10.1021/acs.chemrev.9b00223>.

491 Xie, S., Liu, L., Lu, Y., Wang, C., Cao, S., Diao, W., Deng, J., Tan, W., Ma, L., Ehrlich, S.N.,
492 Li, Y., Zhang, Y., Ye, K., Xin, H., Flytzani-Stephanopoulos, M., Liu, F., 2022. Pt atomic
493 single-layer catalyst embedded in defect-enriched ceria for efficient CO oxidation. *J. Am.*
494 *Chem. Soc.* 144(46), 21255-21266. <https://doi.org/10.1021/jacs.2c08902>.

495 Xie, S., Liu, Y., Deng, J., Zhao, X., Yang, J., Zhang, K., Han, Z., Dai, H., 2016. Three-
496 dimensionally ordered macroporous CeO₂-supported Pd@Co nanoparticles: Highly active
497 catalysts for methane oxidation. *J. Catal.* 342, 17-26.
498 <https://doi.org/10.1016/j.jcat.2016.07.003>.

499 Xie, S., Wang, Z., Tan, W., Zhu, Y., Collier, S., Ma, L., Ehrlich, S.N., Xu, P., Yan, Y., Xu, T.,
500 Deng, J., Liu, F., 2021. Highly active and stable palladium catalysts on novel ceria–alumina
501 supports for efficient oxidation of carbon monoxide and hydrocarbons. *Environ. Sci.*
502 *Technol.* 55(11), 7624-7633. <https://doi.org/https://doi.org/10.1021/acs.est.1c00077>.

503 Xiong, H., Kunwar, D., Jiang, D., García-Vargas, C.E., Li, H., Du, C., Canning, G., Pereira-
504 Hernandez, X.I., Wan, Q., Lin, S., Purdy, S.C., Miller, J.T., Leung, K., Chou, S.S.,
505 Brongersma, H.H., ter Veen, R., Huang, J., Guo, H., Wang, Y., Datye, A.K., 2021.
506 Engineering catalyst supports to stabilize PdO_x two-dimensional rafts for water-tolerant
507 methane oxidation. *Nat. Catal.* 4(10), 830-839. [https://doi.org/10.1038/s41929-021-00680-](https://doi.org/10.1038/s41929-021-00680-4)
508 [4](https://doi.org/10.1038/s41929-021-00680-4).

509 Ye, J., Xia, Y., Cheng, D.-g., Chen, F., Zhan, X., 2019. Promoting effects of pretreatment on
510 Pd/CeO₂ catalysts for CO oxidation. *Int. J. Hydrog. Energy* 44(33), 17985-17994.
511 <https://doi.org/https://doi.org/10.1016/j.ijhydene.2019.05.099>.

512 Zhang, X., Bi, F., Zhu, Z., Yang, Y., Zhao, S., Chen, J., Lv, X., Wang, Y., Xu, J., Liu, N., 2021.
513 The promoting effect of H₂O on rod-like MnCeO_x derived from MOFs for toluene
514 oxidation: A combined experimental and theoretical investigation. *Appl. Catal. B: Environ.*
515 297, 120393. <https://doi.org/10.1016/j.apcatb.2021.120393>.

516 Zhang, X., Zhang, X., Song, L., Hou, F., Yang, Y., Wang, Y., Liu, N., 2018. Enhanced catalytic
517 performance for CO oxidation and preferential CO oxidation over CuO/CeO₂ catalysts
518 synthesized from metal organic framework: Effects of preparation methods. *Int. J. Hydrog.*
519 *Energy* 43(39), 18279-18288. <https://doi.org/10.1016/j.ijhydene.2018.08.060>.

520 Zhang, Z., Tian, J., Lu, Y., Yang, S., Jiang, D., Huang, W., Li, Y., Hong, J., Hoffman, A.S.,
521 Bare, S.R., Engelhard, M.H., Datye, A.K., Wang, Y., 2023. Memory-dictated dynamics of
522 single-atom Pt on CeO₂ for CO oxidation. *Nat. Commun.* 14(1), 2664.
523 <https://doi.org/10.1038/s41467-023-37776-3>.

524